Hindawi Publishing Corporation
Discrete Dynamics in Nature and Society
Volume 2014, Article ID 793864, 10 pages
http://dx.doi.org/10.1155/2014/793864

Research Article

Torque Split Strategy for Parallel Hybrid Electric Vehicles with an Integrated Starter Generator

Zhumu Fu,[1,2] Aiyun Gao,[3] Xiaohong Wang,[1] and Xiaona Song[1]

[1] *College of Information Engineering, Henan University of Science and Technology, Luoyang 471023, China*
[2] *School of Control Science and Engineering, Shandong University, Jinan 250061, China*
[3] *College of Vehicle and Traffic Engineering, Henan University of Science and Technology, Luoyang 471023, China*

Correspondence should be addressed to Zhumu Fu; fzm1974@163.com

Received 24 July 2014; Accepted 20 August 2014; Published 3 September 2014

Academic Editor: Zhengrong Xiang

This paper presents a torque split strategy for parallel hybrid electric vehicles with an integrated starter generator (ISG-PHEV) by using fuzzy logic control. By combining the efficiency map and the optimum torque curve of the internal combustion engine (ICE) with the state of charge (SOC) of the batteries, the torque split strategy is designed, which manages the ICE within its peak efficiency region. Taking the quantified ICE torque, the quantified SOC of the batteries, and the quantified ICE speed as inputs, and regarding the output torque demanded on the ICE as an output, a fuzzy logic controller (FLC) with relevant fuzzy rules has been developed to determine the optimal torque distribution among the ICE, the ISG, and the electric motor/generator (EMG) effectively. The simulation results reveal that, compared with the conventional torque control strategy which uses rule-based controller (RBC) in different driving cycles, the proposed FLC improves the fuel economy of the ISG-PHEV, increases the efficiency of the ICE, and maintains batteries SOC within its operation range more availably.

1. Introduction

In virtue of their low fuel consumption and emissions, along with the feasibility for both urban and interstate transportation, hybrid electric vehicles (HEVs) have been widely studied during recent years [1–4]. Instead of having one motive power source, HEVs have two or more power sources that can act independently or in combination. Based on the traditional system configuration and composition, HEVs can be classified into the series, parallel, and parallel-series three categories. The parallel hybrid electric vehicle (PHEV) adopts two independent driving systems of the engine and the motor to reduce the deadweight and the manufacturing cost of vehicles, so it is a very promising structure. This paper will study the PHEV with an integrated starter generator (ISG-PHEV).

Improving the fuel economy of an ISG-PHEV can be achieved, which is depending on optimizing its mechanical construction, matching the powertrain parameters, lighting the body, and advancing the internal combustion engine (ICE) efficiency. Since the structure of the designed ISG-PHEV in this paper is more complicated, not only containing a conventional ICE, but also including an ISG and an electric motor/generator (EMG), the more importance is also relying on optimizing the energy control strategy. Because the speed of the ICE is not a controllable variable, the torque becomes only a controllable variable. With the information on the required total driving torque, how to split it among the ICE, the ISG, and the EMG is essential to increase the system efficiency, to minimize the fuel consumption, and to maintain the state of charge (SOC) of the batteries.

Along this line, many torques split control strategies have been proposed for efficient energy usage, which can be classified into four types, such as the rule-based control strategy [5], the global optimal strategy [6, 7], the instantaneous optimization control strategy [8], and the fuzzy logic control strategy [9–11]. The present rule-based control strategy commonly sets the initial value of the parameters by mostly depending on engineering experience and then

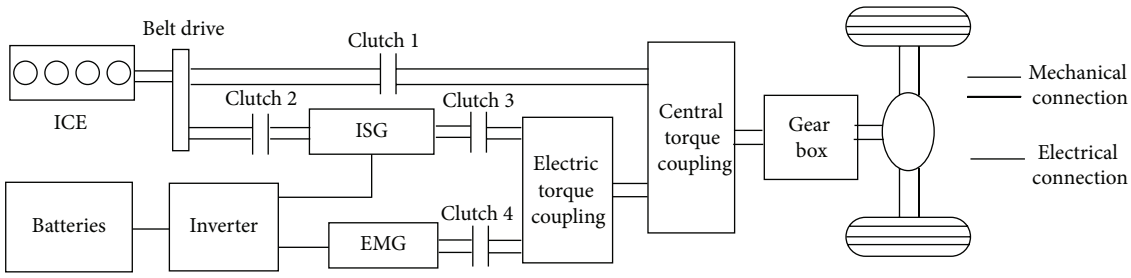

Figure 1: Structure of the ISG-PHEV.

combining the "trial-and-error method" to adjust these parameters. Although this strategy can make a significant improvement in energy efficiency and can be adopted widely in the commercial HEV, it is clear that the strategy does not guarantee an optimal result in all situations or cannot allow the vehicle to reach the maximum efficiency as the fixed parameters [12–14]. The works [6] and [15, 16] propose a global optimal strategy based on dynamic programming methods for the PHEV and the parallel-series HEV, respectively. These techniques can find the global optimal solution of the control parameters with the engine/motor torque. However, they could not offer an online solution because the future driving cycle is assumed entirely known. The works [17–19] propose an instantaneous optimization control strategy based on the equivalent fuel consumption minimization, which considers the total of the ICE's fuel consumption and the batteries' energy consumed at each time. Therein, the batteries' energy consumed is equivalent to the thermal energy of the fuel. The target is to solve the optimizing control variables and to realize the fuel consumption minimization in unknown driving conditions. However, it is difficult to implement the energy control strategy on account of the requirement for intensive computation and precious vehicle models. The fuzzy logic control strategy has been proposed by [20–22] to control the hybrid powertrain, which does not require precise mathematical models, and has both strong robustness and good real-time performance. The fuzzy logic control is the most logical and feasible approach for making decision for an uncertain or imprecise plant and it has already been introduced in many industrial fields. The work [20] utilizes the genetic algorithm to optimize the designed fuzzy controller to improve the fuel economy for driving system of PHEVs. The work [21] uses fuzzy gain scheduling to determine appropriate gains for the PI controller based on the system's operating conditions, which is capable of significantly improving the engine speed and power behavior in a power-split HEV. The work [22] proposes a fuzzy logic energy-management system to make a decision on the power split between the battery and the engine, which controls the engine to work in the vicinity of its maximum fuel efficiency region while preventing the battery from over-discharging. Based on the structure of the designed ISG-PHEV, this paper has developed an innovative logic controller (FLC) by taking more factors into account, which not only ensures that the ICE operates within its peak efficiency region but also obtains high electrical efficiency; thus, the system efficiency is increased obviously while maintaining batteries SOC within its operation range.

In this paper, a torque split strategy based on the fuzzy logic controller (FLC) for PHEV is developed to optimize the operation of all major ISG-PHEV components. The organization of the paper is as follows. Firstly, the ISG-PHEV configuration is introduced and the torque split strategy is briefly described. Subsequently, the design of the FLC is presented. Finally, the simulation results are presented to investigate the effectiveness of the FLC.

2. The Principle of the Torque Split

The structure of the ISG-PHEV is shown in Figure 1. To increase electrical efficiency, the ISG-PHEV adopts two motors including the ISG and the EMG. The ISG is used to start the ICE through a belt, and the EMG is downsized and integrated with the ISG by an electric torque coupling. Both of them can work as driving motor and generator. A central torque coupling connects the ICE with the electric torque coupling, and then the total torque is delivered to the gear box and to the driving wheels. To ensure the independences of the ICE, the ISG, and the EMG, the clutches 1–4 are added.

How to distribute the torque among the ICE, the ISG, and the EMG is very important to obtain the highest efficiency of the ICE. A typical efficiency map of an ICE on the speed-torque plane is shown in Figure 2. The maximum torque curve represents the highest ICE torque achievable for any speed. The contours show constant efficiencies, whose values will increase toward inner contours; therefore, the points in dashed line are the highest efficiency operating points of the ICE at any corresponding speed. The dashed line can be called the ICE optimum torque curve. It is worth noting that the ICE optimum torque curve must be limited within its peak efficiency region ($\eta_{ice} \geq 0.35$); otherwise, the optimal ICE output torque will change suddenly.

When driving the ISG-PHEV, the ICE optimum torque curve is used as a logic threshold value so that the ICE can operate along the optimum torque curve. By neglecting energy losses, the relationships among the ICE, the ISG, and the EMG can be expressed as

$$\begin{aligned} k_1 T_{isg} &= T_{ele} = T_{ice}^{req} - T_{ice}^{opt}, \quad T_{ice}^{opt} > T_{ice}^{req} > 0 \\ k_1 T_{isg} + k_1 k_2 T_{emg} &= T_{ele} = T_{ice}^{req} - T_{ice}^{opt}, \quad \text{else} \end{aligned} \tag{1}$$

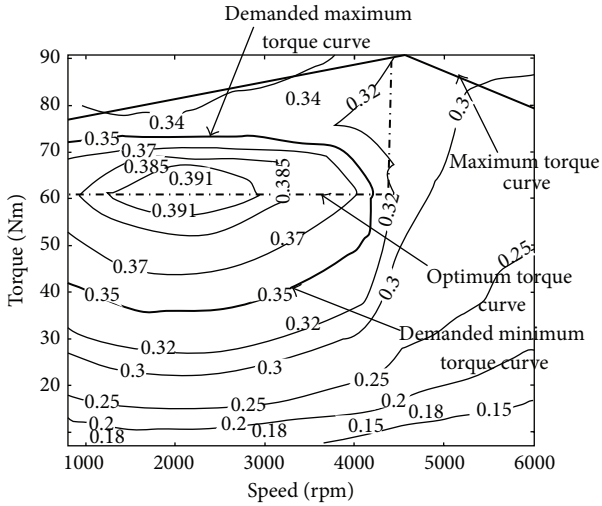

Figure 2: Efficiency map of the ICE operating.

$$\omega_{isg} = k_1\omega_{ice}, \quad T_{ice}^{opt} > T_{ice}^{req} > 0$$
$$\omega_{isg} = k_2\omega_{emg} = k_1k_2\omega_{ice}, \quad \text{else}, \tag{2}$$

where k_1 is the central torque coupling gear ratio; k_2 is the electric torque coupling gear ratio; T_{isg} is the output torque from the ISG; T_{ele} is the output torque of the electrical system; T_{ice}^{req} is the torque demand on the ICE; T_{ice}^{opt} is the optimum output torque of the ICE, when the ICE is stopped, $T_{ice}^{opt} = 0$; T_{emg} is the output torque from the EMG; ω_{isg} is the speed demand on the ISG; ω_{ice} is the actual speed of the ICE, which depends on the ISG-PHEV speed and the gear ratios; and ω_{emg} is the speed demand on the EMG.

Equations (1) and (2) reflect the relationships among the ICE, the ISG, and the EMG when driving the ISG-PHEV. It is easy to calculate the power distribution of every component on the basis of obtaining its torque and speed. For instance, the optimum output power P_{ice}^{opt} from the ICE can be calculated by using T_{ice}^{opt} and optimum output speed ω_{ice}^{opt} of the ICE as follows:

$$T_{ice}^{opt}\omega_{ice}^{opt} = P_{ice}^{opt}. \tag{3}$$

By combining (1) and (3), the output power of the ICE can be controlled at the highest efficiency by changing the output torque of the ISG or the EMG. Since P_{ice}^{opt} is known, the power demand on electrical system can be obtained by

$$P_{ele} = P_{ice}^{req} - P_{ice}^{opt},$$
$$P_{ice}^{req} = T_{ice}^{req}\omega_{ice}, \tag{4}$$

where P_{ele} denotes the power demand on the electrical system and P_{ice}^{req} is the power demand on the ICE.

The power can be distributed between the ISG and the EMG in the electrical system by the known parameter P_{ele}. At a certain speed, when P_{ele} is less than the peak power of the ISG, the electrical power is supplied only by the ISG. While P_{ele} is up to the peak power of the ISG and less than the peak power of the EMG, the electrical power is supplied only by the EMG. Likewise, when P_{ele} is up to the peak power of the EMG, the electrical power is supplied by the ISG and the EMG in combination.

It can be seen that the power among the ICE, the ISG, and the EMG is very easily distributed when using a simple logic threshold approach. However, the ICE may fail to achieve the best efficiency on account of the complex nature of the ISG-PHEV. For example, the nonaccurate models of the ICE, the SOC of the batteries, and the driving cycles are usually important factors affecting the efficiency of the ICE. In this condition, the ICE is operating at the region near the optimum torque curve. The relationships among the ICE, the ISG, and the EMG can be described as

$$k_1T_{isg} = T_{ele} = T_{ice}^{req} - T_{ice}^{act}, \quad T_{ice}^{act} > T_{ice}^{req} > 0$$
$$k_1T_{isg} + k_1k_2T_{emg} = T_{ele} = T_{ice}^{req} - T_{ice}^{act}, \quad \text{else}, \tag{5}$$

where T_{ice}^{act} is the actual output torque of the ICE and $T_{ice}^{act} \geq 0$.

Equation (5) reflects the actual torque distribution among the ICE, the ISG, and the EMG, of which the value T_{ice}^{opt} is very important to design the highest efficiency of the ICE, since it is changed into the actual output torque T_{ice}^{act}, which is related to the SOC of the batteries and the driving cycles.

On the other hand, the fuzzy logic control is a suitable solution for the nonlinear problem. Therefore, in the following, we will design an FLC to achieve the optimization of the ICE output.

3. Design of the FLC

The control system uses an FLC with three inputs and one output, where the first input is the quantified ICE torque, the second input is the quantified SOC, and the third input is the quantified ICE speed. The schematic of control system with an FLC is shown in Figure 3. The quantified ICE torque T_{ice}^{in} and the quantified ICE speed ω are calculated at first. Then, the FLC uses T_{ice}^{in}, ω, and the SOC as inputs to calculate the output demand torque of the ICE (T_{ice}^{dem}). The ICE actual torque T_{ice}^{act} is obtained by measuring the output torque T_{ice}^{dem} and the prejudgment for stop/start of the ICE. Since the sum of the engine and motor torques should be equal to the driver's torque request, the electrical system torque T_{ele} can be calculated. Finally, by combining (5) and the control strategy, T_{isg} and T_{emg} can be obtained.

The design of the FLC must achieve two objectives. One is to make the ICE operate at the suitable points so that it can achieve satisfactory overall system efficiency, and the other is to let the control strategy become more concise and convenient. Hence, the inputs and output should be normalized automatically in order to make the inputs be scaled from 0 to 1 at each time step.

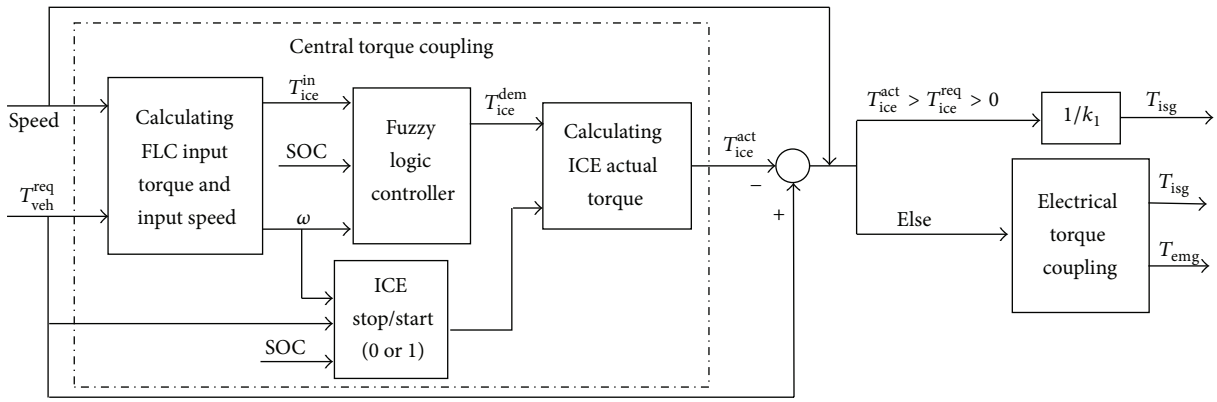

Figure 3: Schematic of control system with an FLC.

3.1. Scaling of Inputs and Output for the FLC. The ICE optimum torque curve is not enough to achieve satisfactory overall system efficiency. The actual torque contribution from the ICE should be determined in a manner such that the driver's torque request is satisfied consistently and the batteries are sufficiently charged at all times. Therefore, the suitable points of the ICE are related to the peak efficiency region and optimum torque curve of the ICE. On the other hand, the driver's torque request, the driving cycles, and the SOC of batteries are also considered to calculate the suitable points of the ICE.

As shown in Figure 2, to make the ICE operate at peak efficiency region ($\eta_{ice} \geq 0.35$), the maximum torque and the minimum torque should be limited within its peak efficiency region. So the demanded maximum torque curve is designed as actual maximum torque curve, and the demanded minimum torque curve is designed as actual minimum torque curve. The ICE optimum torque curve is used in order to scale the range for quantified ICE torque T_{ice}^{in}. On this occasion, the fuzzy input torque value 0.5 corresponds to the optimum torque at each time step. The scaling of quantified ICE torque T_{ice}^{in} is calculated as follows:

$$T_{ice}^{in} = 0.5 \times \frac{T_{ice}^{req} - T_{ice}^{min}}{T_{ice}^{opt} - T_{ice}^{min}}, \quad T_{ice}^{req} \leq T_{ice}^{opt},$$
$$T_{ice}^{in} = 0.5 + 0.5 \times \frac{T_{ice}^{req} - T_{ice}^{opt}}{T_{ice}^{max} - T_{ice}^{opt}}, \quad T_{ice}^{req} > T_{ice}^{opt}, \tag{6}$$

where T_{ice}^{min} is the minimum torque corresponding to demanded minimum torque curve and T_{ice}^{max} is the maximum torque corresponding to demanded maximum torque curve.

How to scale the range for the quantified ICE torque from 0 to 1 is illustrated by (6). In the same way, the quantified SOC and the quantified ICE speed are also normalized automatically. The resistance and the voltage curves corresponding to SOC of the single NI-MH battery used in this study are shown in Figure 4. For this case, the target value of SOC is set to 0.5, the lowest SOC to 0.2, and the highest SOC to 0.8. In SOC scaling for fuzzy input, the method is similar to (6). In the circumstances, 0.5 represents the optimum target value, 0 represents the lowest SOC, and 1 represents the highest SOC.

Let us consider the quantified ICE speed. At any particular point in time, we can get the ICE speed by the current gear ratio and the driving cycles, so we use the ICE speed as the input of the FLC. On the other hand, when we limit the smallest ICE power input designed as 6 KW to ensure the efficiency of the ICE, we design the smallest ICE speed as 800 rpm. And the ICE optimum torque curve must be limited within its peak efficiency region ($\eta_{ice} \geq 0.35$); the biggest speed is designed as 4100 rpm on the basis of Figure 2. At last, the speed 2200 rpm corresponding to the most efficiency of the ICE point is designed as the target value. While in the speed scaling for fuzzy input, 0.5 represents the middle value 2200 rpm, 0 expresses the smallest ICE speed 800 rpm, and 1 means the biggest speed 4100 rpm.

Similarly, the scaling of the fuzzy output is exactly parallel to that of the fuzzy input. In the demand torque scaling for the fuzzy output, 0.5 represents the optimum torque value, 0 stands for the minimum torque value, and 1 delegates the maximum torque value.

3.2. Membership Functions and Fuzzy Rules. The membership functions of inputs and output are shown in Figure 5. All the membership functions use two opening trapezoidal membership functions in the two sides and use a triangular membership function in the middle. Notice that the region of the triangular membership function of the input speed and the output torque is different. The density of the ICE efficiency contours is different in the two sides near the 2100 rpm; the density decreases toward left and increases toward right. So the region of triangular membership function is wider in the left than in the right. On the other hand, we need the output torque which is nearer to the optimum torque curve. The region of triangular membership function of the ICE output torque is narrower than others.

After designing the membership functions, the rules of the FLC are designed. The rules would be modified by observing the control surfaces determined by the inputs and output. In addition, the rules of the FLC should be further modified based on the simulation results. The fuzzy rules of the FLC and their explanations are shown in Table 1. The control surfaces are shown in Figure 6.

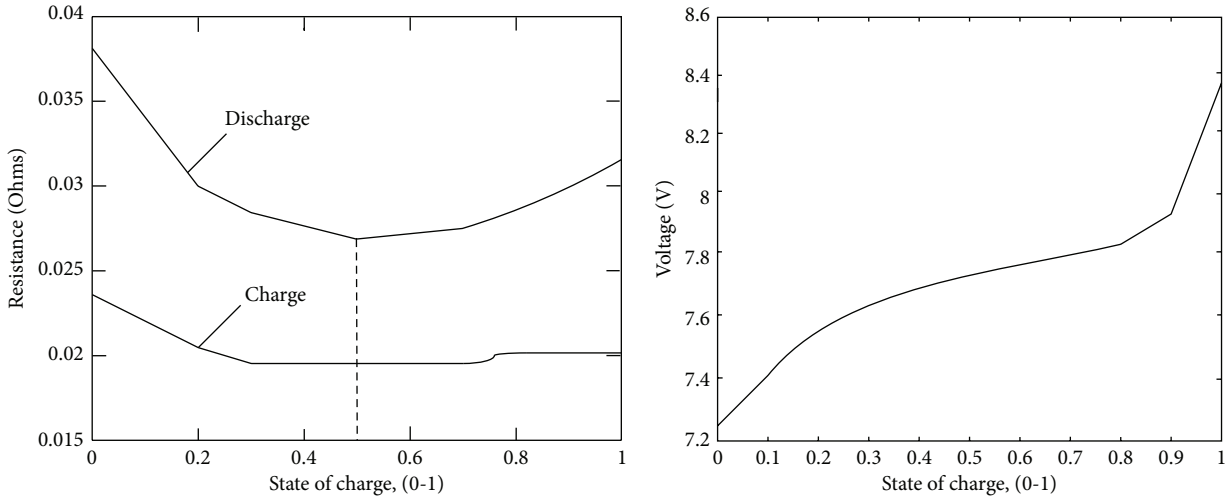

(a) The resistance curves

(b) The voltage curve

Figure 4: The resistance and the voltage curves correspond to the SOC of the NI-MH battery.

Table 1: The fuzzy rules of the FLC.

Rule number	Input torque	SOC	Speed	Output torque	Explanation
1	Low	Low	Low	Opt	Idle speed to mid-speed condition: but battery needs charge, so the output torque should be opt
2	Low	Low	Mid	Opt	
3	Low	Low	High	High	SOC is low, high-speed condition: output torque should be up to opt
4	Low	Target	Low	Low	Battery does not need charging: output torque holds on low
5	Low	Target	Mid	Opt	Speed is mid: output torque should be opt to obtain most efficiency
6	Low	Target	High	High	High-speed condition: output torque should be up to opt
7	Low	High	Low	Low	SOC is high: battery needs discharging, and output torque should be low
8	Low	High	Mid	Low	
9	Low	High	High	Opt	High-speed condition: output torque should be up to low
10	Opt	Low	Low	Opt	Battery does not need discharging, low-speed or mid-speed condition: the output torque is determined by input torque
11	Opt	Low	Mid	Opt	
12	Opt	Low	High	High	Battery need charging, and high-speed condition: output torque should be high
13	Opt	Target	Low	Opt	Battery can be charged or discharged, so the electrical system can provide positive or negative torque for ICE. To obtain most efficiency, output torque should be opt
14	Opt	Target	Mid	Opt	
15	Opt	Target	High	Opt	
16	Opt	High	Low	Low	Battery need discharging, and low-speed condition: output torque should be low
17	Opt	High	Mid	Opt	Battery need discharging, and mid-speed condition: the electrical system can provide positive torque for ICE, so output torque should be opt
18	Opt	High	High	Opt	
19	High	Low	Low	High	The electrical system can not provide positive torque for ICE, so the output torque is determined by input torque
20	High	Low	Mid	High	
21	High	Low	High	High	
22	High	Target	Low	Opt	The electrical system can provide positive torque for ICE. To obtain most efficiency, output torque should be opt
23	High	Target	Mid	Opt	
24	High	Target	High	High	High-speed and high-torque condition
25	High	High	Low	Low	Battery need discharging, and low-speed condition: output torque should be low
26	High	High	Mid	Opt	The electrical system can provide positive torque for ICE. To obtain most efficiency, output torque should be opt
27	High	High	High	Opt	

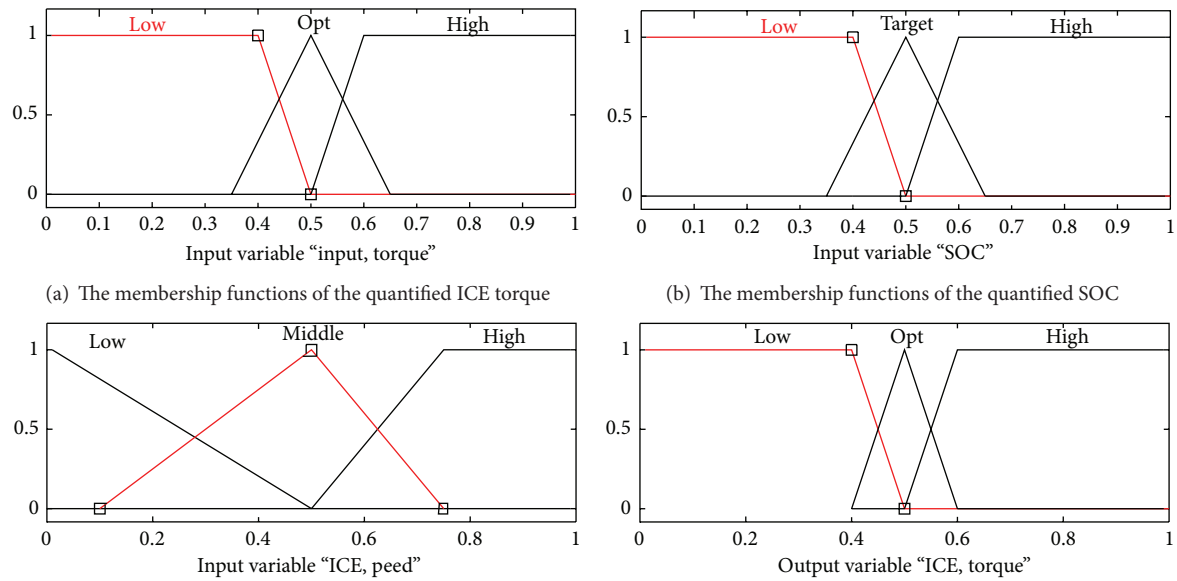

(a) The membership functions of the quantified ICE torque

(b) The membership functions of the quantified SOC

(c) The membership functions of the quantified ICE speed

(d) The membership functions of the output ICE torque

Figure 5: The membership functions of inputs and output.

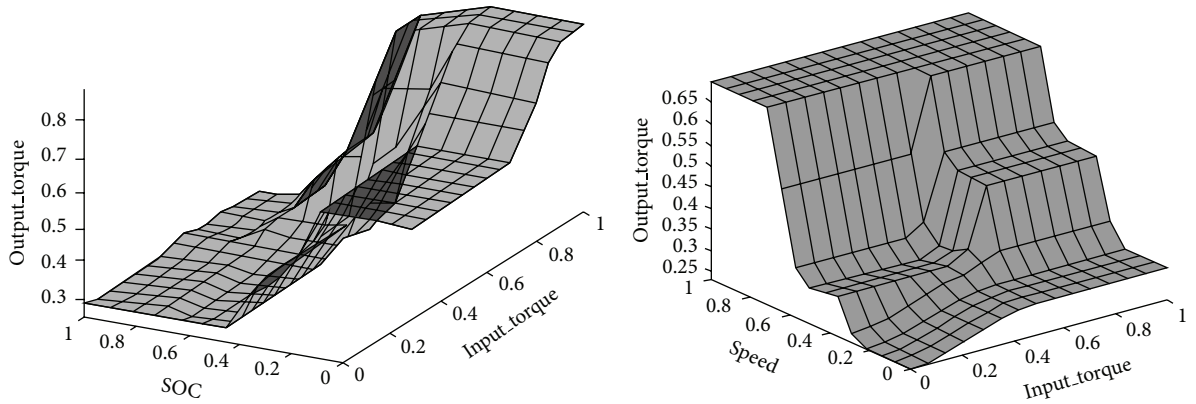

(a) Control surfaces of output torque with input torque and SOC

(b) Control surfaces of output torque with input torque and speed

Figure 6: Control surfaces.

In this paper, through experiences and simulations, the logical AND has been implemented with the minimum operator, the implication method is minimum, the aggregation method is maximum, and the defuzzification method is centroid method.

3.3. Calculating the Actual Torque Distributed in Every Component. It needs to be scaled back later to fit the actual output torque. The actual output torque is calculated as follows:

$$T_{\text{ice}}^{\text{act}} = 2 \times T_{\text{ice}}^{\text{dem}} \left(T_{\text{ice}}^{\text{opt}} - T_{\text{ice}}^{\text{min}}\right) + T_{\text{ice}}^{\text{min}}, \quad T_{\text{ice}}^{\text{req}} \le T_{\text{ice}}^{\text{opt}}$$

$$T_{\text{ice}}^{\text{act}} = 2 \times \left(T_{\text{ice}}^{\text{dem}} - 0.5\right)\left(T_{\text{ice}}^{\text{max}} - T_{\text{ice}}^{\text{opt}}\right) + T_{\text{ice}}^{\text{opt}}, \quad T_{\text{ice}}^{\text{req}} > T_{\text{ice}}^{\text{opt}}. \tag{7}$$

In addition to the above conditions, the actual torque is also related to the stop/start of the ICE, which is determined by the ISG-PHEV speed, the required torque, and the SOC. When the SOC is up to 0.8, the ICE must be stopped. When the SOC is less than 0.2, the ICE must be started. When the SOC is in the region [0.2 0.8], the stop/start of the ICE is indicated by a binary variable, which is expressed as follows:

$$e(t-1) = 0, \qquad e(t) = \begin{cases} 1, & 0.2 \le \text{SOC} \le 0.4 \\ 0, & \text{else} \end{cases}$$

$$e(t-1) = 1, \qquad e(t) = \begin{cases} 0, & 0.6 \le \text{SOC} \le 0.8 \\ 1, & \text{else,} \end{cases} \tag{8}$$

where $e(t)$ is the binary variable; $e(t) = 0$ indicates that the ICE stops and the actual output torque is 0; and $e(t) = 1$ indicates that the ICE starts. The actual output torque can be interpreted as the multiplication of $T_{\text{ice}}^{\text{act}}$ and $e(t)$.

Table 2: Parameters of vehicles.

Component	Parameter	ISG-PHEV value
ICE (Honda-insight)	Peak power	50 kw
	Optimum torque	61 Nm
	Peak efficiency	0.4
EMG (insight)	Peak power	30 kw
	Peak torque	±150 Nm
ISG (insight)	Peak power	10 kw
	Peak torque	±50 Nm
NIHM battery	Voltage	288 V
	Capacity	6.5 Ah
ISG-PHEV data	Radius of wheel	0.275 m
	Frontal area	1.92 m^2
	Total mass	1350 kg

When we get T_{ice}^{act}, we can obtain the electrical system torque demand T_{ele} by combining (5) and Figure 3. When $T_{ele} > 0$ or $T_{ice}^{act} = 0$, in order to distribute the torque between the ISG and the EMG, we define a variable K to achieve the distribution. It is shown as follows:

$$K = \frac{P_{isg}}{P_{ele}}, \tag{9}$$

where P_{isg} is the power contribution of the ISG and P_{ele} is the electrical power demand. So the power contribution of the EMG can be calculated as

$$P_{emg} = (1 - K) P_{ele}. \tag{10}$$

How to calculate the K is very important to obtain the best efficiency of the electrical system. The efficiency of electrical system can be calculated as

$$\begin{aligned} \eta_{ele} &= \left\{ \frac{T_{isg}\omega_{isg}\eta_{isg}^{i} + T_{emg}\omega_{emg}\eta_{emg}^{i}}{P_{isg} + P_{emg}} \right\}^{i} \\ &= \left\{ \frac{P_{isg}\eta_{isg}^{i} + P_{emg}\eta_{emg}^{i}}{P_{isg} + P_{emg}} \right\}^{i}, \end{aligned} \tag{11}$$

where η_{ele} is the efficiency of the electrical system; η_{isg}^{i} is the efficiency of the ISG, $\eta_{isg}^{i} = f(T_{isg}, \omega_{isg})$; and η_{emg}^{i} is the efficiency of the EMG, $\eta_{emg}^{i} = f(T_{emg}, \omega_{emg})$. Here, $i = 1$ indicates that the ISG and the EMG work in the charge state, whereas $i = -1$ means that they work in the discharge state.

By combining (10) and (11), the best efficiency η_{elemax} of the electrical system can be calculated as

$$\eta_{elemax} = \arg\max_{K \in (K_{min}, K_{max})} \left\{ K\eta_{isg}^{i} + (1 - K)\eta_{emg}^{i} \right\}^{i}, \tag{12}$$

where K is varied between the lower limit K_{min} and the upper limit K_{max}. Here, K_{min} and K_{max} are determined by the minimum and maximum power of the ISG and the EMG.

From (11), the output power of ISG and EMG is closely related to their torque and speed, so η_{isg}^{i} and η_{emg}^{i} can be calculated by knowing their output power and speed. For a particular K, the power of the ISG and the EMG can be calculated by (9) and (10). It can be seen from Figure 3 that the speed of the ISG and the EMG also can be obtained by the ISG-PHEV speed corresponding to the driving cycles; thus, we can get the best efficiency of the electrical system. At the same time, we can get the K corresponding to η_{elemax}.

4. Simulation and Comparative Analysis

The new European driving cycle (NEDC), Urban dynamometer driving schedule (UDDS), and economic commission of Europe cycle (CYC_ECE, the ECE cycle is an urban driving cycle, also known as UDC) are chosen to demonstrate the FLC. The important parameters of the ISG-PHEV are listed in Table 2.

And the performance of the ICE in the ISG-PHEV is shown in Figure 7. It is not difficult to find that the operating points of the ICE with the rule-based controller (RBC) are less efficiency. RBC's output torque is higher than expected, especially in the lower speed area or in the starting of the ICE, and some points even reach its maximum torque and exceed the peak efficiency region. However, the out torque of the ICE with the FLC is normal in the region near the optimum torque curve. Its operating points not only behave in the peak efficiency region but also work closer to the optimum torque curve than ones with the RBC.

The comprehensive results of the ISG-PHEV with RBC and FLC in UDDS are compared in Figure 8. It shows that the SOC values begin at 0.7 and finish at 0.51 when operating with RBC. The fluctuation is 0.19. With FLC, the SOC values begin at 0.7 and finish at 0.59. The fluctuation is 0.11. The SOC is well controlled within the desired limits during the driving cycle in comparison with the results obtained from RBC, and the circulation charging/discharging of the batteries has been realized in a balance obviously. Also, it is observed that, using FLC, the output torque of the ICE is more stable and the output torque of the ISG changes bigger than that of RBC, which reflects that the ISG heavily supports the ICE to work along the optimum torque curve. When the electrical system responds to high regenerative braking torque, the ISG and the EMG work in harmony since the variable K is used to achieve the torque distribution between the ISG and the EMG.

To have more specific comparative analysis, the ICE efficiency, the variation of SOC, and the fuel consumption in three driving cycles are shown in Table 3. It is seen that FLC improves the efficiency of the ICE and reduces the variation of SOC. In particular, compared with RBC, the FLC can also reduce the fuel consumption up to 3.7% (in NEDC or UDDS) and 3.1% (in CYC_ECE).

5. Conclusions

In this paper, the FLC for the ISG-PHEV has been presented. This torque controller optimizes the energy flow among the main components of the ICE, the ISG, the EMG, and the batteries for the ISG-PHEV. The FLC manages the operating

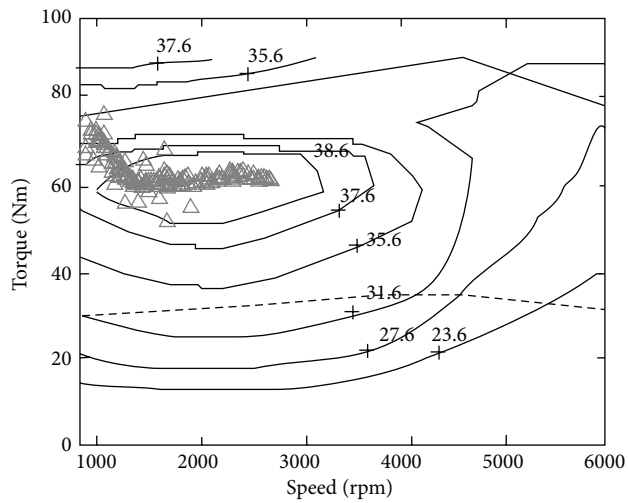

(a) Operating points of the ICE with RBC in NEDC

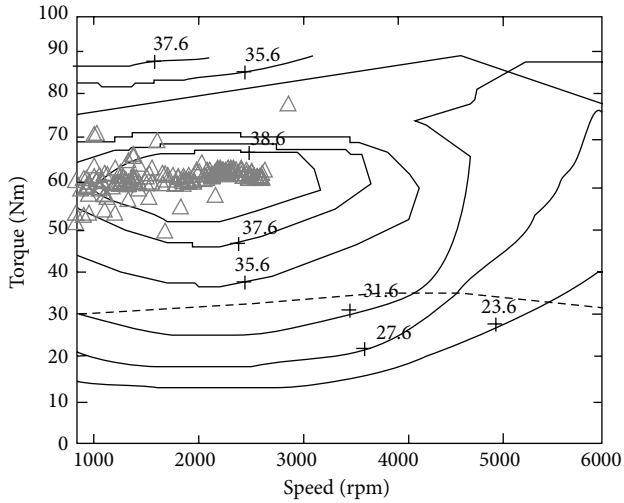

(b) Operating points of the ICE with FLC in NEDC

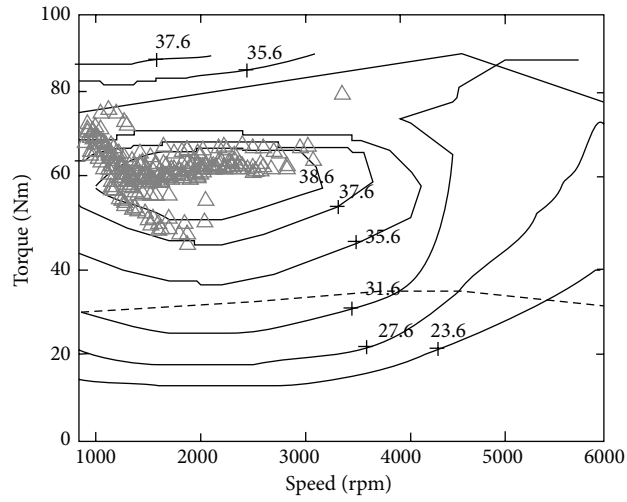

(c) Operating points of the ICE with RBC in UDDS

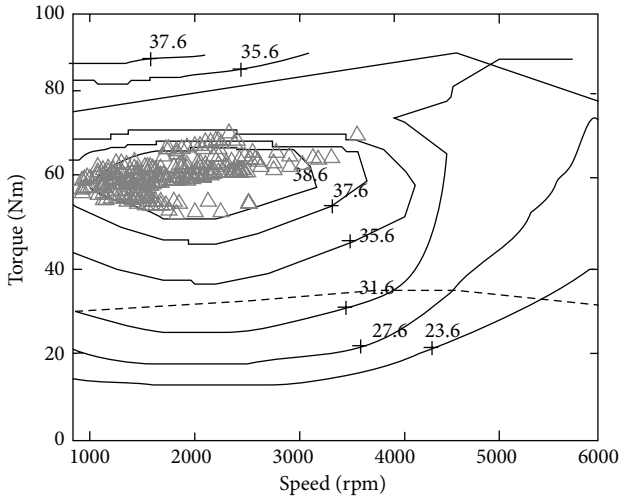

(d) Operating points of the ICE with FLC in UDDS

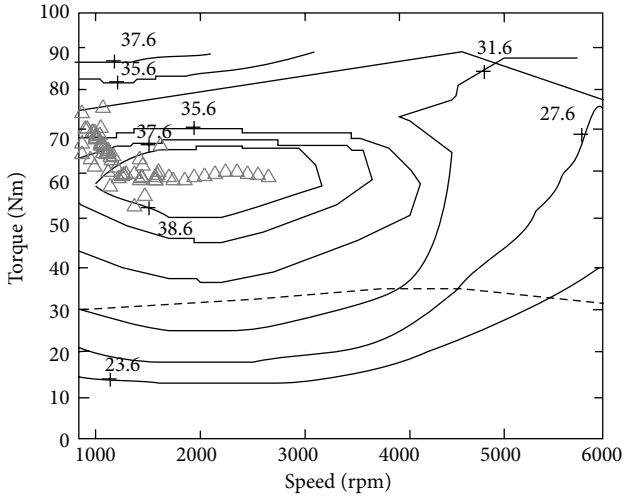

(e) Operating points of the ICE with RBC in ECE

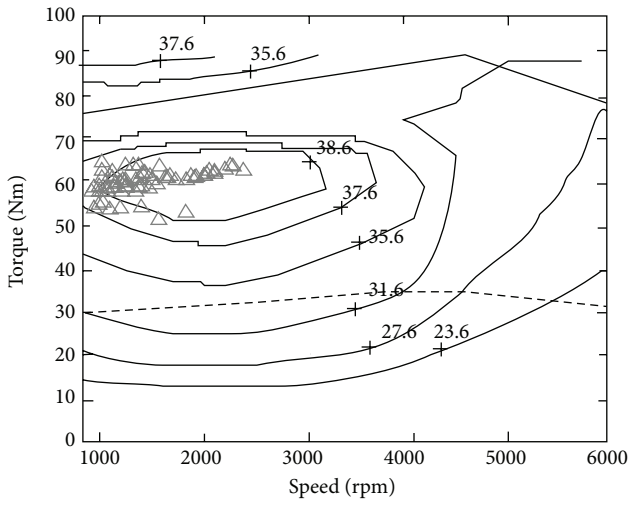

(f) Operating points of the ICE with FLC in ECE

Figure 7: Comparison of simulation.

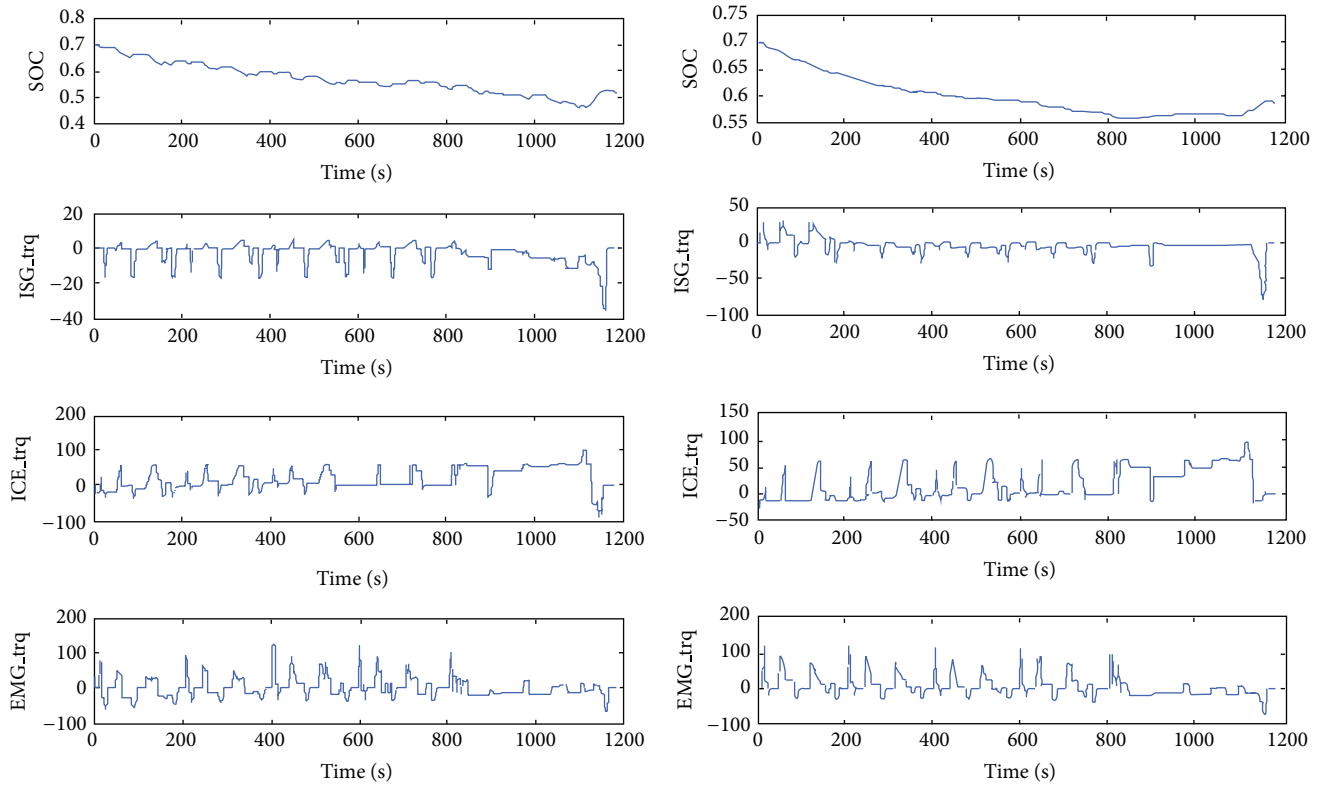

(a) Comprehensive results with RBC

(b) Comprehensive results with FLC

Figure 8: Comprehensive results in UDDS.

Table 3: Comparison of simulation results.

Drive cycle	The ICE efficiency		The variation of the SOC (initial SOC~final SOC)		Fuel consumption (L/100 km)	
	With FLC	With RBC	With FLC	With RBC	With FLC	With RBC
NEDC	37.8%	36.8%	0.60~0.52	0.60~0.47	3.36	3.49
UDDS	36.9%	35.7%	0.60~0.47	0.60~0.4	3.62	3.76
CYC_ECE	37.6%	36.5%	0.60~0.54	0.60~0.51	3.41	3.52

points of the ICE to obtain good fuel economy while still keeping the SOC of the batteries in a proper range.

Simulation results have shown that the ICE efficiency is improved and the variation of the SOCand the fuel consumption of the ISG-PHEV with the FLC are reduced, compared with the conventional torque control strategy which uses RBC in different driving cycles. At the same time, the operating points of the ICE with the FLC not only behave in peak efficiency region but also run closer to the ICE optimum torque curve. The comprehensive results show that the fuel consumption of the ISG-PHEV reduces up to 3.7% (in NEDC or UDDS) and 3.1% (in ECE). These results demonstrate the effectiveness and the validity of the FLC.

In future research, the efficiency of the ISG and the EMG is also taken into account in the design of the FLC to further enhance the fuel economy of the vehicles. Adaptive fuzzy logic strategy will be added to the controller to obtain favorable performances in every driving cycle.

Conflict of Interests

The authors declare that there is no conflict of interests regarding the publication of this paper.

Acknowledgments

The authors would like to thank the anonymous reviewers for their constructive and insightful comments for further improving the quality of this note. This work was partially supported by National Natural Science Foundation of China under Grant nos. 61473115, 61203047, 51277116 and 51375145, China Postdoctoral Science Foundation under Grant 2013T60670, Science and Technology Innovative Foundation for Distinguished Young Scholar of Henan Province under Grant 144100510004, the Science and Technology Programme Foundation for the Innovative Talents of Henan Province University under Grant 13HASTIT038,

and the Key Scientific and Technological Project of Henan Province under Grant 132102210247.

References

[1] S. G. Wirasingha, R. Gremban, and A. Emadi, "Source-to-wheel (STW) analysis of plug-in hybrid electric vehicles," *IEEE Transactions on Smart Grid*, vol. 66, no. 8, pp. 10–20, 2011.

[2] M. Alizadeh, A. Scaglione, J. Davies et al., "A scalable stochastic model for the electricity demand of electric and plug-in hybrid vehicles," *IEEE Transactions on Smart Grid*, vol. 5, no. 2, pp. 848–860, 2014.

[3] F. L. Mapelli, D. Tarsitano, and M. Mauri, "Plug-in hybrid electric vehicle: modeling, prototype realization, and inverter losses reduction analysis," *IEEE Transactions on Industrial Electronics*, vol. 57, no. 2, pp. 598–607, 2010.

[4] S. Kermani, R. Trigui, S. Delprat, B. Jeanneret, and T. M. Guerra, "PHIL implementation of energy management optimization for a parallel HEV on a predefined route," *IEEE Transactions on Vehicular Technology*, vol. 60, no. 3, pp. 782–792, 2011.

[5] E. Vinot and R. Trigui, "Optimal energy management of HEVs with hybrid storage system," *Energy Conversion and Management*, vol. 76, pp. 437–452, 2013.

[6] F. Guo, E. Inoa, W. Choi, and J. Wang, "Study on global optimization and control strategy development for a PHEV charging facility," *IEEE Transactions on Vehicular Technology*, vol. 61, no. 6, pp. 2431–2441, 2012.

[7] R. M. Patil, Z. Filipi, and H. K. Fathy, "Comparison of supervisory control strategies for series plug-in hybrid electric vehicle powertrains through dynamic programming," *IEEE Transactions on Control Systems Technology*, vol. 22, no. 2, pp. 502–509, 2014.

[8] L. Wang, E. G. Collins Jr., and H. Li, "Optimal design and real-time control for energy management in electric vehicles," *IEEE Transactions on Vehicular Technology*, vol. 60, no. 4, pp. 1419–1429, 2011.

[9] A. A. Abdelsalam and S. Cui, "A fuzzy logic global power management strategy for hybrid electric vehicles based on a permanent magnet electric variable transmission," *Energies*, vol. 5, no. 4, pp. 1175–1198, 2012.

[10] J. Wu, C.-H. Zhang, and N.-X. Cui, "Fuzzy energy management strategy for a hybrid electric vehicle based on driving cycle recognition," *International Journal of Automotive Technology*, vol. 13, no. 7, pp. 1159–1167, 2012.

[11] A. Sciarretta, L. Serrao, P. C. Dewangan et al., "A control benchmark on the energy management of a plug-in hybrid electric vehicle," *Control Engineering Practice*, vol. 29, pp. 287–298, 2014.

[12] L. Serrao, S. Onori, and G. Rizzoni, "A comparative analysis of energy management strategies for hybrid electric vehicles," *Journal of Dynamic Systems, Measurement and Control, Transactions of the ASME*, vol. 133, no. 3, Article ID 031012, 2011.

[13] M. Sorrentino, G. Rizzo, and I. Arsie, "Analysis of a rule-based control strategy for on-board energy management of series hybrid vehicles," *Control Engineering Practice*, vol. 19, no. 12, pp. 1433–1441, 2011.

[14] K. Van Berkel, T. Hofman, B. Vroemen, and M. Steinbuch, "Optimal control of a mechanical hybrid powertrain," *IEEE Transactions on Vehicular Technology*, vol. 61, no. 2, pp. 485–497, 2012.

[15] T. Nüesch, A. Cerofolini, G. Mancini et al., "Equivalent consumption minimization strategy for the control of real driving NOx emissions of a diesel hybrid electric vehicle," *Energies*, vol. 7, no. 5, pp. 3148–3178, 2014.

[16] C. Mansour and D. Clodic, "Dynamic modeling of the electro-mechanical configuration of the Toyota Hybrid System series/parallel power train," *International Journal of Automotive Technology*, vol. 13, no. 1, pp. 143–166, 2012.

[17] V. Sezer, M. Gokasan, and S. Bogosyan, "A novel ECMS and combined cost map approach for high-efficiency series hybrid electric vehicles," *IEEE Transactions on Vehicular Technology*, vol. 60, no. 8, pp. 3557–3570, 2011.

[18] N. Kim, S. W. Cha, and H. Peng, "Optimal equivalent fuel consumption for hybrid electric vehicles," *IEEE Transactions on Control Systems Technology*, vol. 20, no. 3, pp. 817–825, 2012.

[19] P. Tulpule, V. Marano, and G. Rizzoni, "Energy management for plug-in hybrid electric vehicles using equivalent consumption minimisation strategy," *International Journal of Electric and Hybrid Vehicles*, vol. 2, no. 4, pp. 329–350, 2010.

[20] A. Poursamad and M. Montazeri, "Design of genetic-fuzzy control strategy for parallel hybrid electric vehicles," *Control Engineering Practice*, vol. 16, no. 7, pp. 861–873, 2008.

[21] S. G. Li, S. M. Sharkh, F. C. Walsh, and C. N. Zhang, "Energy and battery management of a plug-in series hybrid electric vehicle using fuzzy logic," *IEEE Transactions on Vehicular Technology*, vol. 60, no. 8, pp. 3571–3585, 2011.

[22] F. U. Syed, M. L. Kuang, M. Smith, S. Okubo, and H. Ying, "Fuzzy gain-scheduling proportional-integral control for improving engine power and speed behavior in a hybrid electric vehicle," *IEEE Transactions on Vehicular Technology*, vol. 58, no. 1, pp. 69–84, 2009.